

First order $0/\pi$ quantum phase transition in the Kondo regime of a superconducting carbon nanotube quantum dot

Romain Maurand,¹ Tobias Meng,² Edgar Bonet,¹ Serge Florens,¹ Laëtitia Marty,¹ and Wolfgang Wernsdorfer¹

¹*Institut Néel, CNRS et Université Joseph Fourier, BP 166, F-38042 Grenoble Cedex 9, France*

²*Institut für Theoretische Physik, Universität zu Köln, Zùlpicher Str. 77, 50937 Köln, Germany*

(Dated: November 19, 2018)

We study a carbon nanotube quantum dot embedded into a SQUID loop in order to investigate the competition of strong electron correlations with proximity effect. Depending whether local pairing or local magnetism prevails, a superconducting quantum dot will respectively exhibit positive or negative supercurrent, referred to as a 0 or π Josephson junction. In the regime of strong Coulomb blockade, the 0 to π transition is typically controlled by a change in the discrete charge state of the dot, from even to odd. In contrast, at larger tunneling amplitude the Kondo effect develops for an odd charge (magnetic) dot in the normal state, and quenches magnetism. In this situation, we find that a first order 0 to π quantum phase transition can be triggered at fixed valence when superconductivity is brought in, due to the competition of the superconducting gap and the Kondo temperature. The SQUID geometry together with the tunability of our device allows the exploration of the associated phase diagram predicted by recent theories. We also report on the observation of anharmonic behavior of the current-phase relation in the transition regime, that we associate with the two different accessible superconducting states. Our results ultimately reveal the spin singlet nature of the Kondo ground state, which is the key process in allowing the stability of the 0 -phase far from the mixed valence regime.

PACS numbers: 72.15.Qm, 73.21.-b, 73.63.Fg, 74.50+r

I. INTRODUCTION

Realizing a Josephson junction with a carbon nanotube as a weak link opened up the way to a new class of nanoelectronic devices combining both quantum confinement at the nanoscale and the Josephson effect^{1–16}. In these junctions the critical current could be first thought to be maximized when a discrete electronic level of the quantum dot comes into resonance with the Cooper pair condensate of the electrodes, thus allowing an electrostatic tuning of the magnitude of the critical current¹⁷. The Josephson effect in quantum dots is however more complex, because it is governed by the interplay of electronic pairing and strong Coulomb interaction on the dot^{18–28}. When superconductivity dominates, the superconductor wave function spreads over the dot, inducing a BCS-singlet ground state, *i.e.* a standard Josephson junction (dubbed the 0 -state in what follows)¹⁷. In the other extreme regime of large electron-electron interactions, the quantum dot enters the Coulomb blockade domain, and its charge is locked to integer values, altering the superconducting state. For an odd occupancy, quantum dots behave like a spin $S = 1/2$ magnetic impurity that competes with Cooper pair formation, and the ground state can become a magnetic doublet. In this situation, dissipationless current mainly transits through a fourth order tunneling process reordering the spins of Cooper pairs, thus leading to a negative sign of the supercurrent, which is referred to as the π -type Josephson junction^{3,4,29}. These two antagonist superconducting states, associated with a sharp sign reversal of the dissipationless current at zero temperature, can hence allow a first order quantum phase transition by tuning the micro-

scopic parameters in the quantum dot. In the case of very strong Coulomb blockade, the 0 - π transition is achieved by modifying the parity of the electronic charge on the dot (valence is easily changed using electrostatic gates), so that the supercurrent sign reversal occurs at the edges of the Coulomb diamonds. A more intriguing regime occurs for intermediate Coulomb repulsion (associated to moderately small values of the tunneling amplitude compared to the charging energy), in which Kondo correlations take place: in the normal state, the magnetic impurity of the odd charge state is screened through spin-flip cotunneling processes³⁰, providing a non-zero density of states at Fermi energy. This so-called Kondo resonance allows the Cooper pairs to flow normally in the superconducting state, and a 0 -type Josephson junction is therefore recovered^{15,16,19,23,24}. Here we explore in detail how superconducting transport is affected by the presence of Kondo behavior and we finely tune the 0 - π quantum phase transition in this more complex regime by controlling the quantum dot microscopic parameters.

II. CHARACTERIZATION OF THE NANOSQUID

A. Sample fabrication

Here we investigate supercurrent reversal in a carbon nanotube Josephson junction using the nano-SQUID geometry, which implements two Josephson junctions in parallel built with a unique carbon nanotube⁴. The single-wall carbon nanotubes were obtained using laser ablation and then dispersed in a pure dichloroethane

solution using low power ultrasounds. A degenerately doped silicon wafer with a 450nm layer of SiO₂ on top was used as backgate. A first optical lithography step provided alignment marks in order to locate the nanotubes by scanning electron microscopy. The superconducting loops and the sidegates were fabricated using aligned e-beam lithography, followed by e-beam evaporation of Pd/Al bilayer (with respective thickness 4nm/50nm). All measurements were performed in a dilution refrigerator with a base temperature of $T = 35\text{mK}$, and the filtering stages were similar to the ones performed in Ref. 4. Samples were current-biased, either for DC or lock-in measurements (with an AC amplitude of 10pA), in order to measure directly the switching current or the differential resistance of the device. The nano-SQUID switching currents I_{sw} were detected *via* a digital filter which monitors the estimated variance of the average DC voltage, see Appendix C and Ref. 31. Fig. 1a shows a SEM micro-

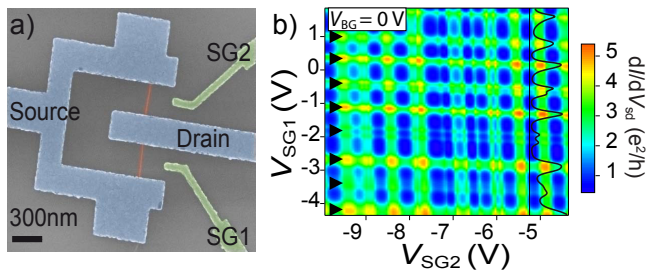


FIG. 1: **Nano-SQUID characteristics.** **a)** SEM micrograph of the measured nano-SQUID. The two sidegates (SG1,SG2) are colored in green, the nanotube defining two quantum dots is shown in red, and the superconducting leads are in blue. **b)** Map of the normal state zero bias conductance dI/dV_{sd} vs the two sidegate voltages at magnetic field $B = 75\text{mT}$, temperature $T = 35\text{mK}$ and backgate voltage $V_{\text{BG}} = 0\text{V}$. Black triangles indicate the odd occupancy regions of the first quantum dot (QD1). A line cut of the linear conductance at fixed $V_{\text{SG}2} = -5.25\text{V}$ is also shown.

graph of the measured nanotube SQUID with two 350nm long nanotube Josephson junctions (JJ1 and JJ2). Using the second quantum dot as a (possibly tunable) reference junction, a precise control over the energy ϵ_0 and linewidth Γ of the first quantum dot is accessible by tuning a pair of local sidegates and a backgate ($V_{\text{SG}1}$, $V_{\text{SG}2}$, V_{BG} respectively), see discussion below. Such a geometry allows us to directly measure the Josephson current of a single junction *via* the magnetic field modulation of the SQUID switching current I_{sw} , see Ref. 4. Indeed, the critical current of an asymmetric SQUID with sinusoidal current-phase relation (taken here for simplicity) can be written as:

$$I_c = \sqrt{(I_{c1} - I_{c2})^2 + 4I_{c1}I_{c2} \left| \cos \left(\pi \frac{\phi}{\phi_0} + \frac{\delta_1 + \delta_2}{2} \right) \right|^2} \quad (1)$$

where ϕ is the flux modulation of the SQUID, $\phi_0 = h/2e$ is the magnetic flux quantum, (δ_1, δ_2) are the intrinsic

phase shifts (0 or π) of the two Josephson junctions, and (I_{c1}, I_{c2}) their respective critical currents. The critical current modulation is thus shifted by $\phi_0/2$ between the $0 - 0$ and the $\pi - 0$ SQUID configuration.

B. Normal state transport properties

Fig. 1b presents the nano-SQUID stability diagram dI/dV_{sd} at zero bias *vs* $V_{\text{SG}1}$ and $V_{\text{SG}2}$ in the normal state (a perpendicular magnetic field of $B = 75\text{mT}$ is applied to suppress superconductivity), at a given backgate $V_{\text{BG}} = 0\text{V}$. This diagram resembles a weakly tilted checkerboard pattern, which is typical for two parallel uncoupled quantum dots in the Coulomb blockade regime, with a weak crosstalk of about 4%. The line-cut at fixed $V_{\text{SG}2} = -5.25\text{V}$ emphasizes the regions of high and low differential conductance associated with the Kondo ridges and Coulomb blocked valleys respectively. One can indeed distinguish easily between even and odd occupancies in each dot from the sequence of conducting and blocked regions: dark blue pockets denote regimes where both dots are blocked (in an even-even configuration of the double dot setup), green lines correspond to the situation of a single dot in the Kondo regime (see arrows) while the other remains blocked (in an even-odd configuration), and red spots show the case where both dots undergo the Kondo effect (in an odd-odd configuration)^{4,30}.

An operating region at a different backgate voltage $V_{\text{BG}} = -0.3\text{V}$ is shown with greater detail on Fig. 2a. For $V_{\text{SG}1}$ between 1.70V and 1.95V, JJ1 has an odd occupancy associated with a differential conductance close to $2e^2/h$ due to a well-developed Kondo effect. Furthermore, JJ2 clearly has an even number of electrons for $V_{\text{SG}2}$ between -4.85V and -5.15V , because of its small contribution to transport in this range. In order to show the influence of the backgate voltage V_{BG} , we have plotted on Fig. 2b the differential conductance *vs* $V_{\text{SG}1}$ for the odd occupancy region of JJ1 corresponding to the white cut on Fig. 2a, taking five different values of V_{BG} from -0.3V to -0.7V . By applying V_{BG} , the sidegates experience a capacitive crosstalk of -21.5% and -17.4% for sidegate 1 and sidegate 2 respectively, as seen by the global shifts of the conductance traces. The application of a backgate voltage thus modifies the occupation number on the dot, but also the tunnel linewidth Γ ^{11,32}. Indeed, by varying the backgate voltage and correcting the sidegates voltages for crosstalk, it is possible to keep the local Coulomb repulsion U and the level position ϵ_0 on the quantum dots relatively constant¹⁶, while the hybridization Γ of the first quantum dot (QD1) experiences sizeable variations up to about 20%, as we discuss now.

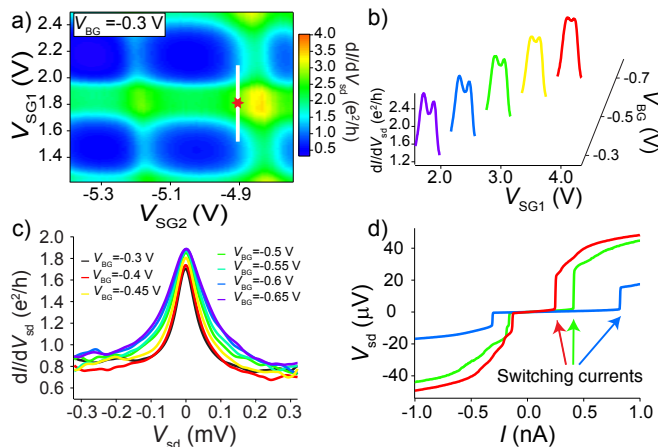


FIG. 2: Kondo correlations and voltage/current characteristics. **a)** Zero bias conductance dI/dV_{sd} vs the sidegate voltages V_{SG1} and V_{SG2} in the normal state (under an applied magnetic field $B = 75\text{mT}$) at $V_{BG} = -0.3\text{V}$, where JJ1 presents a well established Kondo ridge for $1.7\text{V} < V_{SG1} < 1.95\text{V}$ and JJ2 has an even occupancy for $-5.15\text{V} < V_{SG2} < -4.85\text{V}$. **b)** Zero bias dI/dV_{sd} conductance vs sidegate voltage V_{SG1} in the normal state along the white line in panel a) for five different backgate voltages V_{BG} between -0.3V and -0.7V . V_{SG2} was corrected for crosstalk in order to follow the white line, but V_{SG1} was shown as measured. **c)** Finite bias differential conductance dI/dV_{sd} vs source-drain voltage V_{sd} in the normal state, taken in the middle of the Kondo ridge of JJ1 (red star in panel a), corresponding to a level position $\epsilon_0 = 0$) for seven different backgate voltages V_{BG} between -0.7V and -0.3V . The width of the Kondo resonance is modified by the backgate voltage while ϵ_0 and U are kept constant, implying a variation of Γ . **d)** Typical superconducting voltage/current characteristics of the nano-SQUID for three arbitrary values of the gate voltages (V_{SG1}, V_{SG2}). The data are analyzed throughout the paper by recording the switching currents I_{sw} obtained from such voltage/current plot, see Appendix C on the experimental technique that was used.

C. Tuning the hybridization with the gates

On Fig. 2c, the Kondo resonances taken in the middle of the odd occupancy region of QD1 (see corresponding red star in Fig. 2a) are superimposed for different values of V_{BG} . The hybridization Γ can be extracted for different values of the backgate voltage V_{BG} from the half-width at half-maximum V_K of the Kondo resonance in the finite bias conductance. In order to extract systematically V_K , we used a Lorentzian lineshape with fixed background corresponding to the QD2 contribution to transport and to a small elastic cotunneling component for QD1³⁶. Qualitatively, we note the clear increase of V_K that is achieved by shifting the backgate voltage to more negative values, which is related to the gate-induced enhancement of the hybridization Γ reported above. More precisely, in the scaling limit of the Kondo problem³³, a universal behavior of all physical observables is obtained as a function of the Kondo scale, here expressed as a

Kondo voltage V_K :

$$V_K = \alpha \sqrt{\Gamma U} \exp \left[\frac{-\pi U}{8\Gamma} \left(1 - 4 \frac{\epsilon_0^2}{U^2} \right) \right] \quad (2)$$

with U the Coulomb repulsion on the dot, Γ its total hybridization to the leads, and ϵ_0 its energy shift (taken by convention to zero in the middle of the diamond). This expression applies in the limit $U \gg \Gamma$ (for

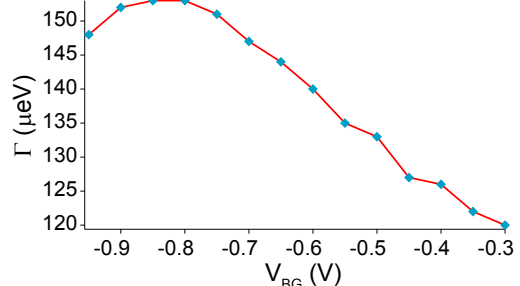


FIG. 3: Hybridization Γ vs backgate voltage V_{BG} . This determination is performed in the middle of the Coulomb diamond of JJ1, see text for details. A control with 20% amplitude variations of Γ is thus achieved by tuning the backgate. For visibility error bars are not indicated here, but are plotted later on Fig. 6.

$-U/2 < \epsilon_0 < U/2$), and contains a yet undetermined prefactor α , which depends on the physical quantity under consideration. To obtain the value of the charging energy U , we have considered the Coulomb stability diagram of JJ1, see Appendix B 1, and extrapolated the diamond edges to large bias. Because of the large linewidth of our strongly coupled nanostructure, the determination of U leads to moderate error bars, and we estimate $U = 0.80 \pm 0.05 \text{ meV}$. Now focusing on the differential conductance dI/dV_{sd} from now on, a more precise definition of α is set by our choice of V_K as the half width at half maximum of the finite-bias Kondo peak. In a near equilibrium situation (corresponding to very asymmetric barrier to the left and right leads) and in the regime $U \gtrsim 6\Gamma$, we find that the unknown parameter is given by $\alpha^{\text{eq}} \simeq 2.8$ from Numerical Renormalization Group (NRG) calculations³⁴. However, in our experiment the conductance is tuned to its maximum value $4e^2/h$ (*i.e.* $2e^2/h$ per dot), corresponding to equally balanced tunneling amplitudes from each leads (we note that values slightly above $4e^2/h$ can be achieved in our double-dot device, which we attribute to small extra elastic contributions from symmetry-broken orbital states of the carbon nanotube). In that case, decoherence of the Kondo anomaly is induced by the antagonist pinning of the Kondo resonance to the split Fermi levels of each lead, reducing the half-width V_K of the finite-bias conductance peak compared to the equilibrium situation. For the relevant regime $U \gtrsim 6\Gamma$, one can estimate³⁵ a reduction by 50% of the linewidth, so that we finally fix $\alpha = 1.4$. Because there is to date no fully controlled theory of the finite bias Kondo resonance, we believe that

the unprecise choice of α will introduce the largest error in our determination of Γ , and hence of the phase boundary analyzed in Sec. III B. The final backgate dependence of the hybridization Γ is shown in Fig. 3 for the middle-point (particle-hole symmetric) of the Coulomb diamond of JJ1. The variations of Γ with the backgate V_{BG} are quite sizeable (up to 20%), according to the exponential dependence of the Kondo scale (2) and constitute a central piece of the analysis in the superconducting state, allowing to span a large part of the phase diagram of the $0-\pi$ transition. We also stress that changing the local sidegates non-only allows to tune the energy levels in the dots, as is clear in Fig. 1b), but also modifies the hybridization Γ . The complete evolution of Γ with backgate and sidegate voltages can be tracked by the analysis of the Kondo anomalies using Eq. (2), and leads to a greater range of variations (up to 50%).

III. EXPERIMENTAL STUDY OF THE FIRST ORDER $0-\pi$ TRANSITION

Having characterized the normal state properties of our device, we now focus on the superconducting behavior of the nano-SQUID. Fig. 2d shows typical voltage-current characteristics obtained at three arbitrary gate voltages in the superconducting state. For all setpoints that we measured, the nano-SQUID shows an abrupt transition to the finite voltage branch indicating an underdamped device, with an hysteretic voltage-current characteristics^{2,4}. The current at which this sharp jump occurs defines the switching current I_{sw} , which can be precisely determined *via* a digital filter³¹ calculating the maximum variance of the measured dc voltage, see Appendix C. Switching currents of approximately 3pA up to a few nA can thus be detected in a fully automated fashion.

A. Comparison between valence induced and Kondo induced $0-\pi$ transition

Here we focus on a comparison of the $0-\pi$ transition behavior in two different correlation regimes, achieved in two distinct regions of the sidegate checkerboard diagram. Fig. 4a and Fig. 4d show both operating regions: a) corresponds to the situation already studied in the normal state, where fully developed Kondo correlations take place for the odd region of JJ1, while d) reveals an odd charge state of JJ1 where Kondo correlations do not arise (Kondo temperature smaller than the base temperature of the cryostat). These distinct physical regime are similarly witnessed on panels b) and e), which show the normal state conductance trace along the white line in the conductance maps. In c), Coulomb blockade is fully overcome by the Kondo effect in the odd region of JJ1, while in e) Coulomb blockade is robust throughout the entire gate range. The most interesting comparison

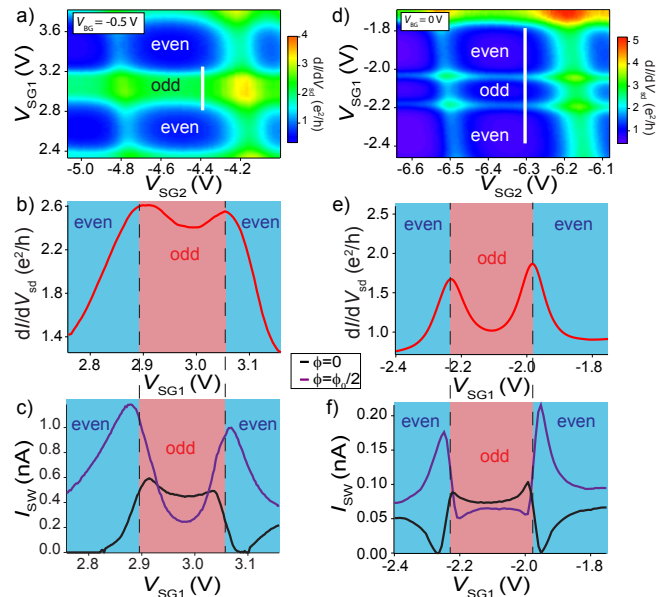


FIG. 4: $0-\pi$ transition in Kondo and Coulomb blocked odd-charge states. Panels a)-b)-c) respectively show the stability diagram, the normal state conductance along the white line in a), and the supercurrent, in the case of a well-developed Kondo effect. Panels d)-e)-f) respectively show the stability diagram, the normal state conductance along the white line in d), and the supercurrent, in the case when Coulomb blockade is not overcome by the Kondo effect. Supercurrent sign reversal, observed by the crossing of the two curves at $\phi = 0$ and $\phi = \phi_0/2$ respectively, penetrates in c) deep within the odd charge Coulomb diamond thanks to Kondo screening, in contrast to f), where the $0-\pi$ crossing occurs precisely when valence changes on the dot.

between the two regimes occurs in the superconducting state, see panels c) and f). In panel c), a supercurrent reversal (indicated by the crossing of the two curves associated to two different magnetic flux, see Eq. 1), occurs *within* the odd charge state of JJ1, showing that the Kondo effect plays a crucial role in triggering the $0-\pi$ transition. In contrast, panel f) shows that the supercurrent changes sign *concomitantly with* the increase of valence of the dot, in agreement with expectations in the strong Coulomb blockade regime²⁹.

B. Tuning the $0-\pi$ transition with controlled changes in the Kondo temperature

As shown in Sec. II C, it is possible to tune the hybridization Γ with the gates, which we exploit to characterize more globally the $0-\pi$ transition phase boundary. Indeed, we saw previously that Kondo correlations in JJ1 are strengthened when V_{BG} goes from $-0.3V$ to $-0.7V$ in the operating region of Fig. 2a. In order to explore precisely the influence of Kondo correlations on the $0-\pi$ transition, Fig. 5 presents six different plots of I_{sw} versus V_{SG1} (along the white line on Fig. 2a) at different

backgate voltages and magnetic fields.

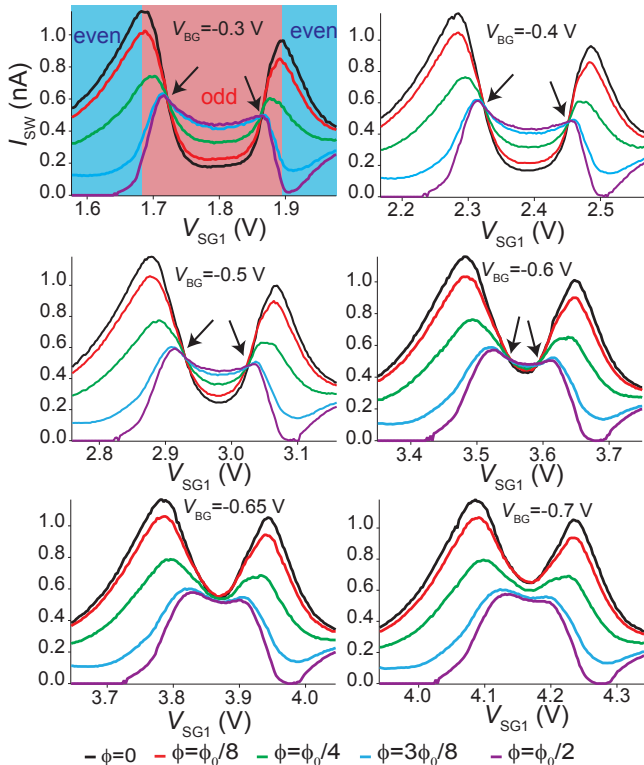


FIG. 5: Switching current behavior of the nano-SQUID in the Kondo regime. The local gate voltage V_{SG1} dependence of the switching current I_{sw} is recorded for five different magnetic fields strengths (plotted as different colored lines). The various panels are displayed by following the decrease of the backgate voltage V_{BG} from -0.3V to -0.7V (the case $V_{BG} = -0.5\text{V}$ was previously shown in Fig. 4a,b,c). This decrease of the backgate voltage allows to strengthen the Kondo effect, progressively shrinking the domain associated to π -junction behavior. Note that V_{SG2} was corrected for crosstalk in order to stay on the white cut shown in Fig. 2a, but the actually measured V_{SG1} is shown here. Arrows denote the transition region between 0 and π -behavior, associated to the crossing point of the switching current.

The traces exhibit two high switching current peaks corresponding to the Coulomb degeneracy points on the sides of the Kondo ridge in an odd valley of QD1. Recording such traces at different magnetic fields provides access to the flux modulation of the switching current in the nano-SQUID. Increasing the magnetic flux ϕ from 0 to $\phi_0/2$ leads to a steady decrease of I_{sw} outside the odd occupancy region of JJ1, which corresponds to a standard 0-type behavior^{3,4} in the Coulomb blocked even valleys of QD1, see Eq. 1. The flux dependence of the switching current within the odd-charge Kondo domain turns out to be more interesting, as we will analyze now. Clearly, the magnetic field behavior of I_{sw} is *reversed* deep inside the odd occupancy region of QD1, as the switching current is greater for $\phi = \phi_0/2$ than for $\phi = 0$, indicating a π -type Josephson behavior. One can therefore iden-

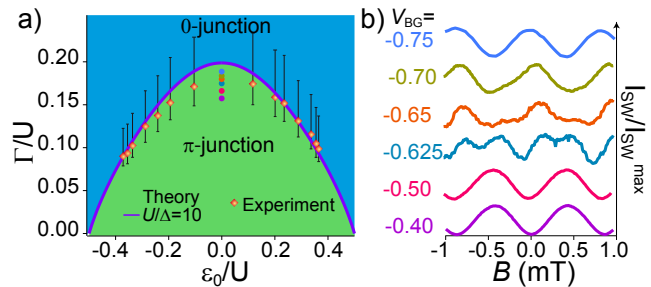


FIG. 6: 0- π phase transition diagram and nano-SQUID modulations. **a)** The experimentally determined phase boundary between 0 and π -junction behavior of JJ1 (orange squares) is given as a function of the dot energy ϵ_0/U and the level width Γ/U . The Coulomb repulsion $U \approx 0.8\text{meV}$ was estimated from the finite bias spectroscopy of the Coulomb blockade diamond. Error bars indicate the uncertainty in the estimate of Γ from the analysis of the Kondo resonances. The purple line represents the theoretical phase diagram for $U/\Delta = 10$ corresponding to the experimental value of $\Delta \approx 80\mu\text{eV}$, see Appendix B 2. **b)** Magnetic field modulations of the nano-SQUID switching current taken in the middle of the odd-charge Kondo ridge (red star in Fig. 2a) for different backgate voltages associated to the fine mesh of dots at $\epsilon_0 = 0$ in panel a). For better comparison, the switching current amplitude, which is strongly suppressed in the transition region. A clear non-harmonic regime occurs near the 0- π phase boundary, where bistable behavior (in phase) of the supercurrent may be attributed to the first order transition between the 0 and π states.

tify precisely from the crossing of the switching current traces at which sidegate voltage V_{SG1} (related to the dot energy) the behavior changes from 0 to π type. This allows to define a 0- π phase boundary for a given backgate voltage. Now, by similarly examining the I_{sw} characteristics at different backgate voltages (allowing to tune the linewidth Γ), we note that decreasing the backgate voltage (*i.e.* enhancing Γ) reduces the range for π behavior, until the π phase completely collapses below the critical $V_{BG} = -0.65\text{V}$ and a 0-junction is maintained all along the Kondo ridge. This physical behavior can be expected from the stronger Kondo screening at larger Γ that tends to favor the 0-state. From these measurements, we can unambiguously assign a 0 or π behavior to the JJ1, as a function of both the level position ϵ_0 and the width Γ of QD1, as determined previously from the analysis of the normal state transport data. For all recorded transitions (corresponding to the black arrows in Fig. 5), we have extracted the corresponding microscopic parameters Γ and ϵ_0 , and plotted them on an experimental phase diagram shown in Fig. 6a. As a quantitative test of our analysis, we have displayed on Fig. 6a the theoretical phase diagram obtained from a self-consistent description of Andreev bound states²⁸ for $U/\Delta \approx 10$ which corresponds to the experimentally measured $U \simeq 0.8\text{meV}$ and $\Delta \simeq 80\mu\text{eV}$. Error bars are taking into account the uncertainty in the determination of

Γ from the finite bias Kondo resonances, see Sec. II C. The bell-shape of the phase boundary together with the nearly quantitative comparison to theory gives strength to the interpretation of the $0-\pi$ transition as a first order phase transition associated to the crossing of the Andreev bound states at the Fermi level^{19,26}. A key point here is that Kondo screening is decisive to allow the existence of the 0 -phase in the center of the odd charge Coulomb diamond in our experimental conditions ($U \simeq 6\Gamma$), see Fig. 7 in Appendix A. While the $0-\pi$ transition is always related to a simple Andreev level crossing, this analysis of our data clearly demonstrates that it is the competition between the normal state Kondo temperature T_K and the superconducting gap Δ which determines the precise location of the $0-\pi$ phase boundary^{26,28}.

From theoretical expectations^{18,27}, a second possible smoking gun for the first order $0-\pi$ phase transition lies in the anharmonic behavior (in phase) of the Josephson junction in close vicinity to the $0-\pi$ phase boundary. This prediction motivates us to consider the field modulation of the switching current I_{sw} with fine changes of the backgate voltage. This is plotted on Fig. 6b, where the quantum dot level was taken in the center of the odd Kondo valley (particle-hole symmetric point $\epsilon_0 = 0$, corresponding to the red star in Fig. 2a and to the fine mesh of dots in Fig. 6a). For $V_{BG} > -0.6V$ modulations show that JJ1 is a π -junction because of the $\phi_0/2$ shift from those of a normal SQUID. On the contrary for $V_{BG} < -0.7V$, modulations turn back to the standard behavior, indicating that JJ1 is a 0 -junction. However, for $-0.6 > V_{BG} > -0.7$ the nano-SQUID switching current modulations show strong anharmonicities. For this range of backgate voltage, the critical current of JJ1 is very small, leading to a strongly asymmetric SQUID, thus JJ2 always switches at the same phase difference, implying that I_{sw} reflects directly the current-phase relation of JJ1³⁷. The observed non-harmonic signal could be interpreted as a further indication for the bistable behavior of the junction associated with the first order $0-\pi$ transition^{18-20,23,27}.

IV. CONCLUSION

In conclusion, we have realized a nano-SQUID based on a superconducting carbon nanotube quantum dots

that is fully tunable thanks a set of electrostatic gates, allowing a precise control of the microscopic parameters of the device. This allowed us to determine an experimental phase diagram for the $0-\pi$ transition in the Kondo regime, which turned in good agreement with theoretical calculations based on the competition between the Kondo temperature and the superconducting gap. The observation of anharmonic behavior in the supercurrent-phase relation near the phase boundary is consistent with the first order nature of the $0-\pi$ transition associated to the crossing of Andreev levels. Fascinating prospects offered by the present work are the control and monitoring of the $0-\pi$ transition from supercurrent measurements, as performed here, with *simultaneous* local spectroscopy of the Andreev spectrum on the quantum dots in the spirit of the recent measurements of Pillet *et al.*³⁸. Such future developments of our experiment, which seems achievable by probing the nano-SQUID with a scanning tunneling microscope, would bring strongly correlated superconducting nanostructures to a new level of control and understanding.

Acknowledgments

We thank T. Crozes, E. Eyraud, D. Lepoittevin, C. Hoarau, and R. Haettel for their technical work, C. Thirion and R. Piquerele for their contributions in programming, and V. Bouchiat, H. Bouchiat, C. Balseiro, J.-P. Cleuziou, L. Bogani, S. Datta, D. Feinberg and T. Novotný for useful discussions. The samples were fabricated in the NANOFAB facility of the Néel Institute. This work is partially financed by ANR-PNANO projects MolNanoSpin No. ANR-08-NANO-002, ERC Advanced Grant MolNanoSpin No. 226558, and STEP MolSpin-QIP.

¹ S. De Franceschi, L. Kouwenhoven, C. Schönberger, and W. Wernsdorfer, *Hybrid superconductor -quantum dot devices*, Nature Nanotech. **5**, 703 (2010).
² P. Jarillo-Herrero, J. A Van Dam, and L. P Kouwenhoven, *Quantum supercurrent transistors in carbon nanotubes*, Nature **439**, 953956 (2006).
³ J. A. Van Dam, Y. V Nazarov, E. P.A.M Bakkers, S. De Franceschi, and L. P Kouwenhoven, *Supercurrent reversal in quantum dots*, Nature **442**, 667 (2006).

⁴ J.-P. Cleuziou, W. Wernsdorfer, V. Bouchiat, T. Ondarçuhu, and M. Monthieux, *Carbon nanotube superconducting quantum interference device*, Nature Nanotech. **1**, 53 (2006).
⁵ C. B. Winkelmann, N. Roch, W. Wernsdorfer, V. Bouchiat, and F. Balestro, *Superconductivity in a single C60 transistor*, Nature Physics **5**, 876 (2009).
⁶ L. Hofstetter, S. Csonka, J. Nygård, and C. Schönberger, *Cooper pair splitter realized in a two-quantum-dot Y-*

- junction* Nature **461**, 960 (2009).
- ⁷ L. G. Herrmann, F. Portier, P. Roche, A. Levy Yeyati, T. Kontos, and C. Strunk *Carbon nanotubes as cooper-pair beam splitters* Phys. Rev. Lett. **104**, 026801 (2010).
 - ⁸ H. Ingerslev Jorgensen, T. Novotny, K. Grove-Rasmussen, K. Flensberg, and P. E Lindelof, *Critical current 0- π transition in designed josephson quantum dot junctions*, Nano Letters **7**, 2441 (2007).
 - ⁹ A. Y. Kasumov, R. Deblock, M. Kociak, B. Reulet, H. Bouchiat, I. I. Khodos, Yu. B. Gorbatov, V. T. Volkov, C. Journet, and M. Burghard, *Supercurrents Through Single-Walled Carbon Nanotubes*, Science **284**, 1508-1511 (1999).
 - ¹⁰ M. R. Buitelaar, T. Nussbaumer, and C. Schonenberger, *Quantum dot in the Kondo regime coupled to superconductors*, Phys. Rev. Lett. **89**, 256801 (2002).
 - ¹¹ J.-P. Cleuziou, W. Wernsdorfer, V. Bouchiat, T. Ondarçuhu, and M. Monthieux, *Tuning the Kondo effect with back and side gates - Application to carbon nanotube superconducting quantum interference devices and pi-junctions*, Preprint arXiv:0610622 (2006).
 - ¹² J.-P. Cleuziou, W. Wernsdorfer, S. Andergassen, S. Florens, V. Bouchiat, T. Ondarçuhu, and M. Monthieux, *Gate-Tuned High Frequency Response of Carbon Nanotube Josephson Junctions*, Phys. Rev. Lett. **99**, 117001 (2007).
 - ¹³ E. Pallecchi, M. Gaass, D. A. Ryndyk, and Ch. Strunk, *Carbon nanotube Josephson junctions with Nb contacts*, Appl. Phys. Lett. **93**, 072501 (2008).
 - ¹⁴ K. Grove-Rasmussen, H. I. Jørgensen, B. M. Andersen, J. Paaske, T. S. Jespersen, J. Nygrd, K. Flensberg, and P. E. Lindelof, *Superconductivity-enhanced bias spectroscopy in carbon nanotube quantum dots*, Phys. Rev. B **79**, (2009).
 - ¹⁵ A. Eichler, R. Deblock, M. Weiss, C. Karrasch, V. Meden, C. Schonenberger, and H. Bouchiat, *Tuning the Josephson current in carbon nanotubes with the Kondo effect*, Phys. Rev. B **79**, (2009).
 - ¹⁶ Y. Kanai, R. S. Deacon, A. Oiwa, K. Yoshida, K. Shibata, K. Hirakawa, and S. Tarucha, *Electrical control of Kondo effect and superconducting transport in a side-gated InAs quantum dot Josephson junction*, Phys. Rev. B **82**, 54512 (2010).
 - ¹⁷ C. W. J. Beenakker, and H. van Houten, *Single-Electron Tunneling and Mesoscopic Devices* (Springer, Berlin, 1992).
 - ¹⁸ A. V. Rozhkov and D. P Arovas, *Josephson coupling through a magnetic impurity*, Phys. Rev. Lett. **82**, 2788 (1999).
 - ¹⁹ A. A. Clerk, and V. Ambegaokar, *Loss of π -junction behavior in an interacting impurity Josephson junction*, Phys. Rev. B **61**, 9109 (2000).
 - ²⁰ T. Yoshioka, and Y. Ohashi, *Numerical renormalization group studies on single impurity Anderson model in superconductivity: a unified treatment of magnetic, nonmagnetic impurities, and resonance scattering*, J. Phys. Soc. Japan **69**, 1812 (2000).
 - ²¹ E. Vecino, A. Martin-Rodero, and A. Levy Yeyati, *Josephson current through a correlated quantum level: Andreev states and π junction behavior* Phys. Rev. B **68**, 035105 (2003).
 - ²² F. Siano, and R. Egger, *Josephson current through a nanoscale magnetic quantum dot*, Phys. Rev. Lett. **93**, 047002 (2004).
 - ²³ M. S. Choi, M. Lee, K. Kang, and W. Belzig, *Kondo effect and Josephson current through a quantum dot between two superconductors*, Phys. Rev. B **70**, 020502 (2004).
 - ²⁴ G. Sellier, T. Kopp, J. Kroha, and Y. S. Barash, *π -Junction behavior and Andreev bound states in Kondo quantum dots with superconducting leads*, Phys. Rev. B **72**, 174502 (2005).
 - ²⁵ Tomas Novotny, Alessandra Rossini, and Karsten Flensberg, *Josephson current through a molecular transistor in a dissipative environment*, Phys. Rev. B **72**, 224502 (2005).
 - ²⁶ J. Bauer, A. Oguri, and A. C. Hewson, *Spectral properties of locally correlated electrons in a Bardeen-Cooper-Schrieffer superconductor*, J. Phys.: Condens. Matter **19**, 486211 (2007).
 - ²⁷ C. Karrasch, A. Oguri, and V. Meden, *Josephson current through a single Anderson impurity coupled to BCS leads*, Phys. Rev. B **77**, 024517 (2008).
 - ²⁸ T. Meng, S. Florens, and P. Simon, *Self-consistent description of Andreev bound states in Josephson quantum dot devices*, Phys. Rev. B **79**, 224521 (2009).
 - ²⁹ L. I. Glazman, and K. A. Matveev, *Resonant Josephson current through Kondo impurities in a tunnel barrier*, JETP Lett. **49**, 659 (1989).
 - ³⁰ L. Kouwenhoven, and L. Glazman, *Revival of the Kondo effect*, Phys. World **14**, 33 (2001).
 - ³¹ Liu, W. Y., Magnin, I. E. & Gimenez, G. *A New Operator for the Detection of Transitions in Noisy Signals*, Traitement du Signal **12**, 225 (1995).
 - ³² H. Grabert, and M. H. Devoret, *Single Charge Tunneling*, Plenum press, New York, 1992.
 - ³³ F. D. M. Haldane, *Scaling Theory of the Asymmetric Anderson Model*, Phys. Rev. Lett. **40**, 416 (1978).
 - ³⁴ R. Bulla, T. A. C. Costi, and T. Pruschke, *Numerical renormalization group method for quantum impurity systems*, Rev. Mod. Phys. **80**, 395 (2008).
 - ³⁵ T. Fujii, and K. Ueda, *Perturbative approach to the nonequilibrium Kondo effect in a quantum dot*, Phys. Rev. B **68**, 1 (2003).
 - ³⁶ D. Goldhaber-Gordon, J. Gres, M. Kastner, Hadas Shtrikman, D. Mahalu, and U. Meirav, *From the Kondo Regime to the Mixed-Valence Regime in a Single-Electron Transistor*, Phys. Rev. Lett. **81**, 5225 (1998).
 - ³⁷ M. Della Rocca, M. Chauvin, B. Huard, H. Pothier, D. Esteve, and C. Urbina, *Measurement of the Current-Phase Relation of Superconducting Atomic Contacts*, Phys. Rev. Lett. **99**, 127005 (2007).
 - ³⁸ J.-D. Pillet, C. H. L. Quay, P. Morfin, C. Bena, A. Levy Yeyati, and P. Joyez, *Andreev bound states in supercurrent-carrying carbon nanotubes revealed*, Nature Physics **6**, 965 (2010).

Appendix A: Theoretical analysis of the 0 – π phase diagram

1. Model for a superconducting quantum dot

The standard Hamiltonian to describe a single superconducting quantum dot is given by the superconducting Anderson model

$$H = \sum_{i=L,R} H_i + H_d + \sum_{i=L,R} H_{T_i}, \quad (\text{A1})$$

where

$$\begin{aligned}
H_i &= \sum_{\vec{k},\sigma} \epsilon_{\vec{k}} c_{\vec{k},\sigma,i}^\dagger c_{\vec{k},\sigma,i} - \sum_{\vec{k}} \left(\Delta_i c_{\vec{k},\uparrow,i}^\dagger c_{-\vec{k},\downarrow,i}^\dagger + \text{h.c.} \right) \\
H_d &= \sum_{\sigma} (\epsilon_0 + U/2) d_{\sigma}^\dagger d_{\sigma} + U n_{\uparrow} n_{\downarrow} \\
H_{T_i} &= \sum_{\vec{k},\sigma} \left(t d_{\sigma}^\dagger c_{\vec{k},\sigma,i} + \text{h.c.} \right).
\end{aligned}$$

In the above equations, d_{σ} is the annihilation operator of an electron with spin σ on the dot, $c_{\vec{k},\sigma,i}$ that of an electron with spin σ and wave vector \vec{k} in the lead $i = L, R$, and $n_{\sigma} = d_{\sigma}^\dagger d_{\sigma}$. The leads are described by standard s-wave BCS Hamiltonians H_i with superconducting gaps $\Delta_i = \Delta e^{i\varphi_i}$. The phase difference of the latter is noted $\varphi = \varphi_L - \varphi_R$. Furthermore, the leads are assumed to have flat and symmetric conduction bands, i.e. the kinetic energy $\epsilon_{\vec{k},i}$ measured from the Fermi level ranges in $[-D, D]$ and the density of states is $\rho_0 = 1/(2D)$. We assume \vec{k} -independent and symmetric tunneling amplitudes t between the dot and both superconducting leads. The dot is described by a single energy level ϵ_0 submitted to the Coulomb interaction U (in our convention ϵ_0 vanishes at the center of the Coulomb diamond).

2. Renormalized Andreev Bound states and phase diagram of the $0-\pi$ transition

In the superconducting state, the four atomic states of the quantum dot evolve onto renormalized Andreev

bound states (ABS) that possibly live within the gap. A quantitative description of this process was proposed in Ref. 28, starting with bare values of the ABS splitting in the limit of infinite gap:

$$\delta E_-^0 = E_-^0 - E_{\sigma}^0 = \frac{U}{2} - \sqrt{\epsilon_0^2 + \Gamma_{\varphi}^2} \quad (\text{A2})$$

$$\delta E_+^0 = E_+^0 - E_{\sigma}^0 = \frac{U}{2} + \sqrt{\epsilon_0^2 + \Gamma_{\varphi}^2}. \quad (\text{A3})$$

with

$$\Gamma_{\varphi} = \Gamma \frac{2}{\pi} \arctan \left(\frac{D}{\Delta} \right) \cos \left(\frac{\varphi}{2} \right). \quad (\text{A4})$$

In this simplified (and unrealistic) limit, the $0/\pi$ transition corresponds to the crossing of the $|-\rangle$ and $|\sigma\rangle$ states, which occurs for $\delta E_-^0 = 0$, leading to a dome-like shape in the $(\epsilon_0/U, \Gamma/U)$ plane. However, the phase boundary quantitatively depends on the precise value of the superconducting gap Δ , which must be more realistically included in the calculation. This is done by calculating the corrections at order $1/\Delta$ to the ABS positions²⁸, followed by a self-consistency loop that takes into account the leading logarithmic singularities:

$$\begin{aligned}
\delta E_-(\Delta) &= \delta E_-^0 - \frac{\Gamma}{\pi} \int_0^D d\epsilon \left[\frac{2}{E - \delta E_-(\Delta)} - \frac{1}{E + \delta E_+^0} - \frac{1}{E + \delta E_-^0} \right. \\
&\quad \left. + \frac{2\Delta}{E} uv \left| \cos \left(\frac{\varphi}{2} \right) \right| \left(\frac{2}{E - \delta E_-(\Delta)} - \frac{1}{E + \delta E_+^0} + \frac{1}{E + \delta E_-^0} \right) \right] + 2|\Gamma_{\varphi}| uv
\end{aligned} \quad (\text{A5})$$

and

$$\begin{aligned}
\delta E_+(\Delta) &= \delta E_+^0 - \frac{\Gamma}{\pi} \int_0^D d\epsilon \left[\frac{2}{E - \delta E_+(\Delta)} - \frac{1}{E + \delta E_+^0} - \frac{1}{E + \delta E_-^0} \right. \\
&\quad \left. + \frac{2\Delta}{E} uv \left| \cos \left(\frac{\varphi}{2} \right) \right| \left(\frac{-2}{E - \delta E_+(\Delta)} - \frac{1}{E + \delta E_+^0} + \frac{1}{E + \delta E_-^0} \right) \right] - 2|\Gamma_{\varphi}| uv,
\end{aligned} \quad (\text{A6})$$

with $E = \sqrt{\epsilon^2 + \Delta^2}$, and $\delta E_-^0, \delta E_+^0$ have been defined in Eqs. (A2)-(A3). The numerical resolution of the self-consistent equation (A5) provides an accurate determination of the phase boundary under the condition $\delta E_-(\Delta) = 0$, that we successfully compared to the experimental data. Note that we corrected here a misprint

in Ref. 28, namely a factor 2 in front of the second term within the integral in (A5)-(A6).

In order to stress the key role of the Kondo effect for the $0-\pi$ transition in our experimental conditions, we compare the phase diagram at particle-hole symmetry ($\epsilon_0 = 0$) obtained from the renormalized-ABS the-

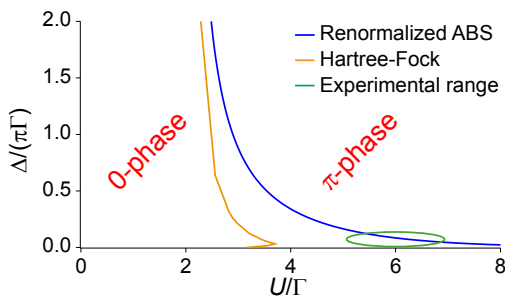


FIG. 7: **Theoretical phase diagram for the 0- π transition at particle-hole symmetry.** A comparison between the renormalized-ABS theory (which includes Kondo correlations) and static Hartree-Fock theory is made. Computations were done for the large bandwidth limit of the superconducting Anderson model Eq. (A1), and the experimental range of the operating region of Figs. 5 and 6 was added for clarity. This comparison shows the key role of Kondo screening to allow the existence of a 0- π transition at intermediate correlations ($U > \pi\Gamma$).

ory²⁸ and from *static* Hartree-Fock mean-field theory¹⁸, see Fig. 7. Because the renormalized-ABS approach includes the Kondo scale (at one-loop order), it allows the extension of the 0- π boundary for arbitrary large values of U/Γ . In contrast, the static mean-field approach is unable to restore a 0-state for Coulomb interaction such that $U \gtrsim \pi\Gamma$, and fails to reproduce our experimental observation of a supercurrent reversal in the regime $U \simeq 6\Gamma$. This comparison shows that the phase boundary in our experiment is indeed associated to a competition between the normal state Kondo temperature and the superconducting gap, in agreement with theoretical expectations^{26,28}.

Appendix B: Determination of the microscopic parameters of the nanosquid

1. Charging energy

Because the charging energy U in a carbon nanotube quantum dot results from the confinement between fixed contacts, one does not expect large variations of U for small detuning of the backgate. In order to determine the experimental phase diagram for the 0 - π transition, an estimate of U is required. This is obtained by considering the Coulomb stability diagram of JJ1 for two different values of the backgate, see Fig. 8, and extrapolating the diamond edges to large bias. Because of the large linewidth of our strongly coupled nanostructure, the determination of U also contains sizeable error bars, which we estimate as $U = 0.80 \pm 0.05 \text{ meV}$.

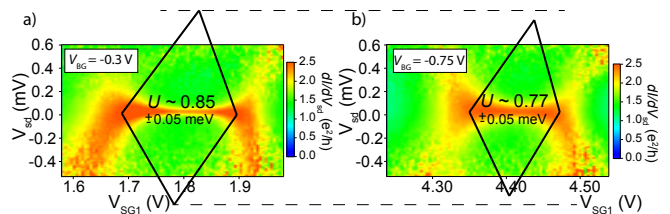


FIG. 8: **Conductance map of JJ1 for two values of the backgate voltage.** Extending the diamond edges to finite bias allows to extract the Coulomb repulsion of the dot $U = 0.80 \pm 0.05 \text{ meV}$.

2. Proximity gap

Current-bias measurements were performed in order to directly access both the superconducting switching current and the differential conductance of the nano-SQUID at $T = 35 \text{ mK}$. In the presence of superconductivity, the two cotunneling peaks associated with quasiparticle current in the differential conductance¹⁰ appear at $V = \pm 2\Delta/e \approx \pm 160 \mu\text{V}$, where 2Δ is the superconducting gap provided by the proximity effect on the nanotube, see Fig. 9. This allows to extract the superconducting gap in our device, $\Delta \approx 80 \mu\text{eV}$, which is reduced from the bulk value of $\Delta_{\text{bulk}} = 175 \mu\text{eV}$ for aluminum, due to the thin palladium contact layer between the carbon nanotube and the aluminum electrodes.

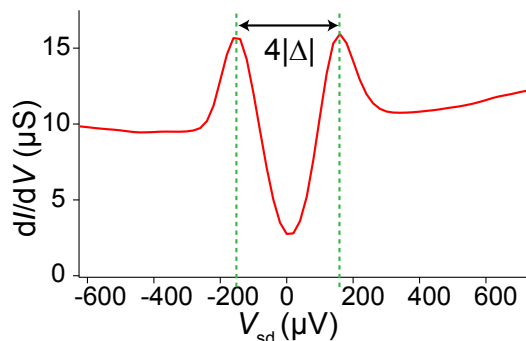


FIG. 9: **Signature of the superconducting 50 nm thick aluminum leads.** The differential conductance *vs* bias voltage shows the presence of a superconducting gap around zero bias, as well as the cotunneling peaks arising from the quasiparticle tunneling. The gap value $\Delta \approx 80 \mu\text{eV}$ is thus obtained. The measurement was done in a blocked region of the nano-SQUID, which explain that no supercurrent is visible at zero bias.

Appendix C: Switching current detection

In order to have an accurate method to extract the switching current from voltage/current characteristics, even for small transition voltage jumps to the dissipative state, we have implemented a digital filter based on the

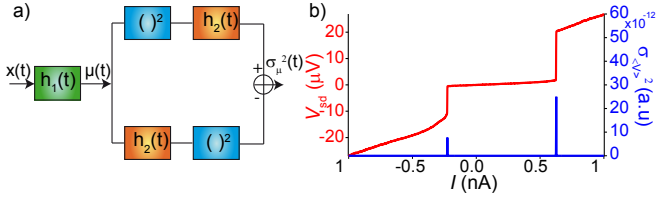


FIG. 10: Digital filter for switching current detection. **a)** Schematic view of the implemented filter based on the work of Liu *et al.*³¹. The first order moment $\mu(t)$ of the signal $x(t)$ in a sliding window is obtained through the filter $h_1(t) = \text{Rect}(t/L_1)/L_1$, with $\text{Rect}(t)$ the normalised rectangular function and L_1 the filter length. The variance $\sigma_\mu^2(t)$ of $\mu(t)$ is simply calculated as $\langle \mu(t)^2 \rangle - \langle \mu(t) \rangle^2$ in a sliding window with $h_2(t) = \text{Rect}(t/L_2)/L_2$. **b)** Voltage/Current characteristics and the estimated variance of the first order moment obtained by the implemented digital filter.

work of Liu *et al.*³¹. The main purpose of this filter is the detection of transitions from noisy signal, which we apply to the superconducting/ normal transition. The operation consists in estimating the variance of the first order moment of the signal in a sliding window. A schematic view of the filter is presented in Fig. 10a. The first order moment $\mu(t)$ is estimated to begin with *via* a classic averaging filter in a sliding window characterized by the impulse response $h_1(t) = \text{Rect}(t/L_1)/L_1$ with $\text{Rect}(t)$ the normalised rectangular function and L_1 the filter length. Finally the estimated variance is obtained by $\langle \mu(t)^2 \rangle - \langle \mu(t) \rangle^2$ with another averaging filter $h_2(t)$ of length L_2 . For the switching current detection with a sample rate of one thousand, we have taken $L_1 = L_2 = 4$. Such filter provides a sharp signal from the steplike features of our voltage/current characteristics as presented in Fig. 10b.